PHYSICAL REVIEW C **90**, 061305(R) (2014)

Evidence of halo structure in ^{37}Mg observed via reaction cross sections and intruder orbitals beyond the island of inversion

M. Takechi,[1,2,3,*] S. Suzuki,[4] D. Nishimura,[5,6] M. Fukuda,[5] T. Ohtsubo,[4] M. Nagashima,[4] T. Suzuki,[7] T. Yamaguchi,[7] A. Ozawa,[8] T. Moriguchi,[8] H. Ohishi,[8] T. Sumikama,[9] H. Geissel,[1] N. Aoi,[2] Rui-Jiu Chen,[2] De-Qing Fang,[10] N. Fukuda,[2] S. Fukuoka,[8] H. Furuki,[7] N. Inabe,[2] Y. Ishibashi,[8] T. Itoh,[4] T. Izumikawa,[4] D. Kameda,[2] T. Kubo,[2] M. Lantz,[2] C. S. Lee,[7] Yu-Gang Ma,[10] K. Matsuta,[5] M. Mihara,[5] S. Momota,[11] D. Nagae,[8] R. Nishikiori,[8] T. Niwa,[8] T. Ohnishi,[2] K. Okumura,[8] M. Ohtake,[2] T. Ogura,[4] H. Sakurai,[2] K. Sato,[7] Y. Shimbara,[3] H. Suzuki,[8] H. Takeda,[2] S. Takeuchi,[2] K. Tanaka,[2] M. Tanaka,[5] H. Uenishi,[5] M. Winkler,[1] Y. Yanagisawa,[2] S. Watanabe,[12] K. Minomo,[12] S. Tagami,[12] M. Shimada,[12] M. Kimura,[13] T. Matsumoto,[12] Y. R. Shimizu,[12] and M. Yahiro[12]

[1]*GSI Helmholtzzentrum für Schwerionenforschung, 64291 Darmstadt, Germany*
[2]*RIKEN, Nishina Center, Wako, Saitama 351-0198, Japan*
[3]*Graduate School of Science and Technology, Niigata University, Niigata 950-2102, Japan*
[4]*Department of Physics, Niigata University, Niigata 950-2102, Japan*
[5]*Department of Physics, Osaka University, Osaka 560-0043, Japan*
[6]*Department of Physics, Tokyo University of Science, Chiba, 278-8510, Japan*
[7]*Department of Physics, Saitama University, Saitama 338-8570, Japan*
[8]*Institute of Physics, University of Tsukuba, Ibaraki, 305-8571, Japan*
[9]*Department of Physics, Tohoku University, Miyagi, 980-8577, Japan*
[10]*Shanghai Institute of Applied Physics, Chinese Academy of Sciences, P. O. Box 800-204, Shanghai 201800, People's Republic of China*
[11]*School of Environmental Science and Engineering, Kochi University of Technology, Kochi, 782-8502, Japan*
[12]*Department of Physics, Kyushu University, Fukuoka 812-8581, Japan*
[13]*Department of Physics, Hokkaido University, Sapporo 060-0810, Japan*

(Received 9 January 2014; revised manuscript received 2 October 2014; published 29 December 2014)

Precise reaction cross sections (σ_R) for $^{24-38}$Mg on C targets at energies around 240 MeV/nucleon have been measured at the Radioactive Isotope Beam Factory at RIKEN. The σ_R for $^{36-38}$Mg have been measured for the first time. An enhancement of σ_R compared to the systematics for spherical stable nuclei has been observed, especially in the neutron-rich region, which reflects the deformation of those isotopes. In the vicinity of the drip line the σ_R for ^{37}Mg is especially large. It is shown by analysis using a recently developed theoretical method that this prominent enhancement of σ_R for ^{37}Mg should come from the p-orbital halo formation breaking the $N = 28$ shell gap.

DOI: 10.1103/PhysRevC.90.061305 PACS number(s): 21.10.Gv, 25.60.Dz

Since the early years of the study of atomic nuclei, the nuclear shell model has been the basic framework for understanding nuclear structure. The high stability of nuclei with certain numbers of neutrons (or protons) observed in stable nuclei indicates the existence of the shells filled at certain so-called "magic numbers." Studies in the last few decades have revealed that those magic numbers are sometimes broken or changed in unstable nuclei [1]. The breakdown of the $N = 20$ shell gap between the sd and fp shells has been extensively studied since the irregularities in binding energies and 2^+ excitation energies were observed in neutron-rich nuclei around $N = 20$ [2–6]. The term "island of inversion" was applied to this region [6] and deformed nuclear structures related to the changing of shell structures have been reported in this region [7]. The vanishing of the $N = 28$ shell closure has been also extensively studied, starting from neutron-rich S-Ar isotopes [8–14]. The development of deformation observed in those nuclei could be interpreted as degeneracy of the fp shell, which induces strong quadrupole deformation [9–11,13–18]. Such deformation has been reported also for Si isotopes [19,20], and studies have recently indicated that this phenomenon could be seen even in a very neutron-rich Mg region [21].

The purpose of our present study is to elucidate the changes of nuclear structures, such as a development of deformation, a breakdown of the magic numbers and possible halo formation in Mg isotopes, from the stability line to the vicinity of the neutron drip line. For this purpose, precise measurements of reaction cross sections for $^{24-38}$Mg have been performed at the Radioactive Isotope Beam Factory (RIBF) at RIKEN. The reaction cross section σ_R or interaction cross section σ_I reflects the nuclear size, and has been a powerful probe in searching for halo formation since the first study by Tanihata *et al.* [22]. Recently, measurements of σ_I for Ne isotopes performed at RIBF [23] have successfully revealed the halo structure of ^{31}Ne in which the sd-pf shell inversion associated with nuclear deformation causes the formation of a halo [23–25]. Moreover, theoretical studies on those data have shown that a precise data set on σ_R is very sensitive indicator of nuclear deformation [23,26,27].

In this Rapid Communication, we report the deformation characteristics of Mg isotopes and a halo formation in ^{37}Mg resulting from the breakdown of the $N = 28$ magic number. The σ_R data have been analyzed by using a newly developed theoretical method [26–28]. Based on this understanding of

*takechi@np.gs.niigata-u.ac.jp

the development of nuclear deformation in Mg isotopes, the anomaly in ^{37}Mg has been revealed. The sudden and large enhancement of σ_R for ^{37}Mg beyond the systematics of other Mg isotopes is analyzed using the deformed Woods-Saxon (DWS) model. The result indicates a low-ℓ orbital halo structure of ^{37}Mg in which the 25th valence neutron is sitting in the p-dominant intruder orbital, which in the conventional shell model is considered to be above the $N = 28$ shell gap.

Experiments were performed at the RIBF operated by the RIKEN Nishina Center and the Center for Nuclear Study, University of Tokyo. A primary beam of ^{48}Ca with a beam energy of 345 MeV/nucleon and a maximum beam current of approximately 100 pnA and Be production targets were used to produce $^{24-38}$Mg secondary beams. σ_R were measured by the transmission method and the BigRIPS fragment separator [29,30] was used as a spectrometer to identify incoming and outgoing particles [23]. A schematic view of the beam line and the experimental setup can be found in Ref. [23]. σ_R is obtained from the relation $\sigma_R = -\frac{1}{t}\ln(\frac{\Gamma}{\Gamma_0})$, where Γ is the ratio of the number of noninteracting outgoing particles to the number of incoming particles, Γ_0 is the same ratio for an empty-target measurement to correct for nuclear reactions in the detectors, and t denotes the thickness of the reaction target. The carbon reaction target of 1.79 or 3.59 g/cm^2 thickness was located at the F5 dispersive focal plane of BigRIPS. The mean energies of secondary beams in the reaction target were approximately 240 MeV/nucleon. Incoming particles were pre-separated and identified using the beam line between the F3 and F5 focal planes, and outgoing particles were identified between the F5 and F7 focal planes. For particle identification before and after the reaction target, magnetic rigidity, energy-loss, and time-of-flight (TOF) information from ion chambers at F3 and F7 and plastic scintillation counters at F3, F5, and F7 were used. The position information from the PPACs at F3 was used to apply an appropriate emittance cut for the incident beam so as to accurately count all of the noninteracting particles without missing them after the reaction target. With this setup, incoming particles can be completely separated from the other fragments and noninteracting outgoing particles can be separated from the other events except for the inelastic scattering events, which have the same atomic and mass numbers but slightly different energies. In the σ_R analysis, the inelastic scattering cross sections ($\sigma_{\rm inel}$) are often extracted from the tail of the energy distribution of the particles [31]. In this work, the TOF and magnetic rigidity distribution of the particles are used to estimate $\sigma_{\rm inel}$. In the insert of Fig. 1(a) deduced $\sigma_{\rm inel}$ are plotted as a function of mass number. The error of σ_R is almost determined by the uncertainty of the estimation of $\sigma_{\rm inel}$, which is shown as the error bar of each $\sigma_{\rm inel}$ datum in the insert. For the case of ^{38}Mg, statistical error is dominant. The yields of ^{37,38}Mg secondary beams, the most neutron-rich nuclei in this work, were 2 particles/s (^{37}Mg) and 1 particle/s (^{38}Mg) with the primary beam intensity of 50 pnA.

The present results of σ_R for $^{24-38}$Mg are plotted as a function of mass number in Fig. 1(a). Especially, the cross section data for $^{36-38}$Mg have been measured for the first time. The σ_R obtained for neutron-rich Mg isotopes including those new data are $\sigma_R(^{34}\text{Mg}) = 1433(18)$ mb, $\sigma_R(^{35}\text{Mg}) = 1443(12)$ mb, $\sigma_R(^{36}\text{Mg}) = 1472(5)$ mb, $\sigma_R(^{37}\text{Mg}) = 1538(15)$ mb, and $\sigma_R(^{38}\text{Mg}) = 1535(21)$ mb. The systematic mass-number dependence of σ_R for stable nuclei is shown by a solid curve for comparison. The dependence was calculated by a Glauber-type calculation (MOL[FM] in Ref. [32]) assuming the nucleon density distributions of the stable nuclei as spherical Fermi distributions (the function and parameters of which are from the same electron scattering data as those described in [23].). Existing experimental σ_R for stable nuclei ^{12}C on a ^{27}Al target measured at a beam energy of 250.7 MeV/nucleon [32] and on a ^{40}Ca target [33] measured at a beam energy of 83 MeV/nucleon, which has been corrected for the energy dependence using MOL[FM] are plotted by open circles for comparison with the systematics for stable nuclei. The present data for Mg isotopes show somewhat larger values compared to the systematics over the whole mass range. The deviation of the data from the systematics tends to be gradually larger with increasing mass number and the enhancement of σ_R for $^{31-38}$Mg is especially large compared to that for $^{24-30}$Mg with smaller neutron numbers.

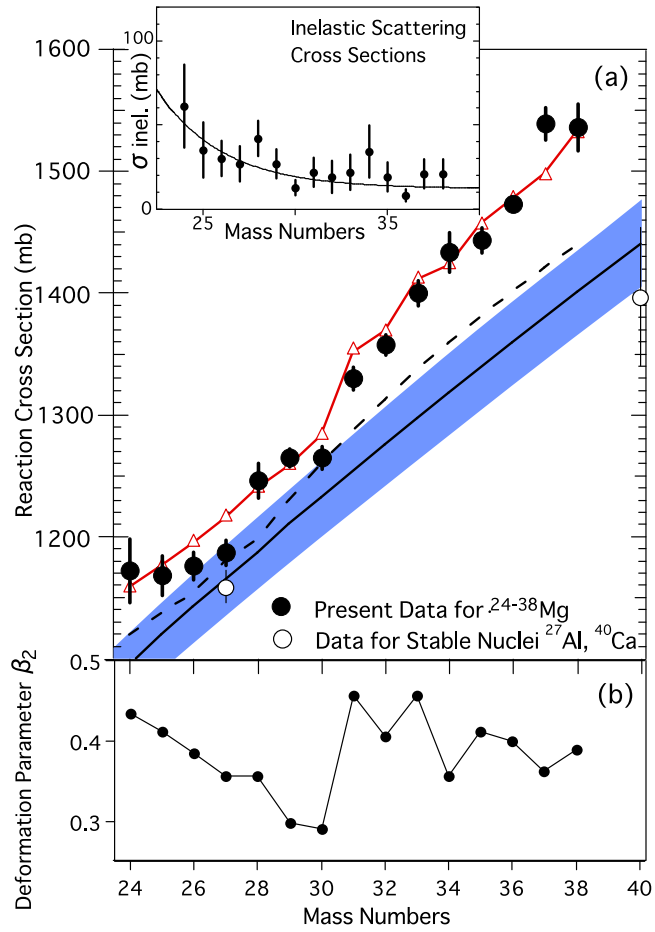

FIG. 1. (Color online) (a) σ_R data for $^{24-38}$Mg (closed circles) plotted against mass number. The DFM calculations (open triangles and dashed line; see text) and the systematics for stable nuclei (thick solid line) are also plotted. The shaded region is the ambiguity of systematics from the fluctuation of electron-scattering data. The insert shows deduced $\sigma_{\rm inel}$ (see text). The curve is to guide the eyes. (b) The deformation parameter β_2 from the AMD calculation is plotted against mass number.

The dashed line in Fig. 1(a) shows the results of the double-folding model (DFM) with the Melbourne-type g-matrix interaction [28,34] in which the projectile densities are obtained by a spherical Hartree-Fock model with the Gogny D1S interaction [35]. The result agrees fairly well with the systematics for stable nuclei but considerably underestimates the present experimental data over the whole mass range. The fact that the DFM calculation can also reproduce σ_R data quite well using reasonable projectile and target densities argues that the densities of the Mg isotopes used in this calculation are inappropriate.

To clarify the source of the trends in the present data, the data were analyzed by the DFM with projectile densities as follows: the mean-field wave functions are constructed by a DWS potential with the deformation parameter evaluated by the antisymmetrized molecular dynamics (AMD) calculation with the Gogny D1S interaction. This AMD calculation has been improved to describe the deformation properties of nuclei and has successfully reproduced the large $B(E2)$ value of ^{32}Mg [36], and successfully applied to the analysis of the cross sections of Ne isotopes with the combination of DFM method [28].

In Fig. 1(a), the result shown by a solid line with open triangles reproduces the data well, and the same prescription has been used with success to reproduce the data for Ne isotopes $^{28-32}$Ne [26–28]. The success of the theoretical calculations in the Mg and Ne isotopes indicates that nuclear deformation is present in these isotopes.

In Fig. 1(b), the deformation parameters β_2 for Mg isotopes deduced by AMD are plotted as a function of mass number. The β_2 of Mg isotopes in this mass range are all positive and decrease from ^{24}Mg to ^{30}Mg, with a sudden sharp increase for ^{31}Mg. The present σ_R data, which cannot be reproduced using the spherical model, seem to be explained by a calculation in which the deformation effect is taken into account. In particular the large enhancement of σ_R for ^{31}Mg is well accounted for by the large deformation indicated by the AMD calculation. This sudden increase of deformation for ^{31}Mg can be understood if there is a border of the island of inversion between $N = 18$ and 19 for Mg isotopes as described in [37].

The DFM calculations are thus quite successful in reproducing the data, and the trends of Mg isotope cross sections can be understood, because they reflect the development of deformation in those nuclei. Recently the trends of σ_R for Mg isotopes related to deformation features have been calculated by using the deformed Skyrme Hartree-Fock (def-SHF) method and Glauber model [38], which also shows good agreement with current DFM calculations despite the difference of theoretical model. In Fig. 1, we can see a deviation from the DFM calculation for ^{27}Mg, which is rather closer to the result of the spherical model. For ^{37}Mg, we can see the largest deviation (by 3σ) and this is a very anomalous result. This result means that while the other Mg isotopes have enhanced size owing to quite well-deformed structure of them, ^{37}Mg suddenly has an even more enhanced size beyond the deformation systematics. The recent work by Kobayashi *et al.* has reported a large Coulomb breakup cross section for ^{37}Mg compared to ^{33}Mg and ^{35}Mg, which might also suggest this anomaly of ^{37}Mg [39,40], and very recently they further discuss and indicate the halo structure of ^{37}Mg also from parallel momentum distribution data [41].

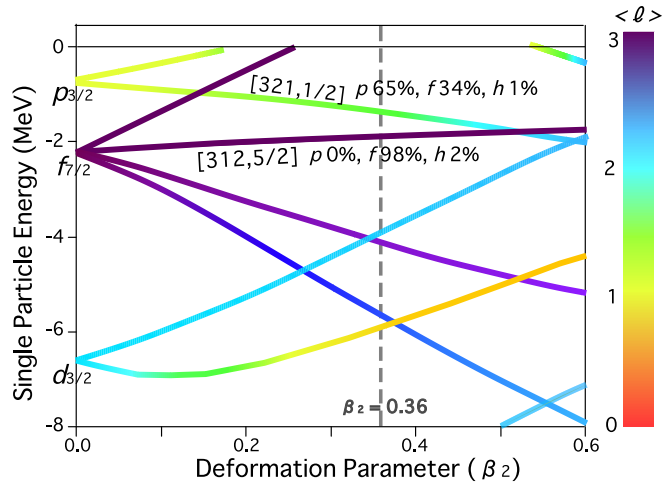

FIG. 2. (Color online) Nilsson diagram calculated with a DWS potential. The expectation value of angular momentum $\langle \ell \rangle$ of orbital is expressed by colors. The darker colors indicate the larger values of $\langle \ell \rangle$ and the lighter colors the smaller values. The deformation parameter for the core of ^{37}Mg from the AMD calculation is indicated by the vertical dashed line. Two candidates for the valence neutron orbital are indicated by their indices [321 1/2] and [312 5/2].

^{37}Mg is a quite exotic nucleus in the vicinity of the neutron drip line. There is an estimated value of one neutron separation energy (S_n) of 0.16 ± 0.68 MeV [42]. Very recently, the value $0.22^{+0.12}_{-0.09}$ MeV has been reported by Kobayashi *et al.*, which was deduced to reproduce their one neutron-removal cross section data on the basis of the Coulomb breakup model [41]. Most of the other Mg isotopes have S_n more than 2 MeV, except for ^{35}Mg for which S_n is 0.75 ± 0.18 MeV [42]. The S_n of ^{37}Mg may be so small that ^{37}Mg can have an extremely weakly bound valence neutron which may form a neutron halo in ^{37}Mg depending on the orbital angular momentum.

In the conventional spherical shell model the valence neutron of ^{37}Mg occupies an $f_{7/2}$ orbital that cannot produce a halo structure. This fact should be considered by taking into account deformation, since the core nucleus ^{36}Mg is well deformed, with $\beta_2 \sim 0.4$ according to the AMD result. Therefore, we analyze the possible orbitals of the valence neutron by using the single-particle model with the deformed Woods-Saxon potential.

Figure 2 shows the Nilsson diagram for ^{37}Mg calculated with the DWS potential as described in [28], in which the single-particle energies are drawn against β_2. The result shown in Fig. 2 is basically equivalent to the diagram in Ref. [43], and here the expectation value of angular momentum $\langle \ell \rangle$ of the orbital is expressed by colors. As for $\beta_2 \sim 0.36$ evaluated with AMD for ^{37}Mg, there are two candidates for the Nilsson orbital that the valence neutron occupies in ^{37}Mg. One is the [312 5/2] orbital from the spherical $0f_{7/2}$ orbital, and the other is the [321 1/2] orbital originating from the spherical $1p_{3/2}$ orbital.

Using the nucleon density distributions extracted with the DWS potential, we calculated the σ_R with the DFM and show the results as a function of S_n in Fig. 3. In this calculation, the

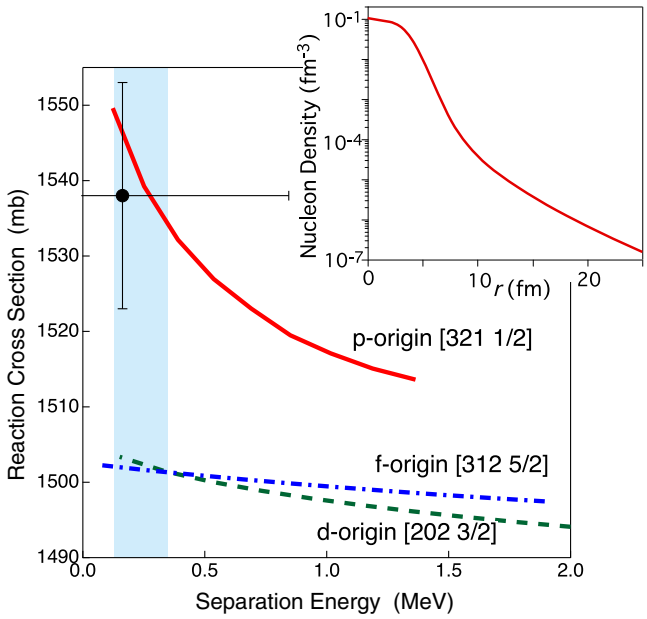

FIG. 3. (Color online) σ_R for ^{37}Mg + ^{12}C at 240 MeV/nucleon calculated with the DFM assuming three types of main orbital for the valence neutron from the DWS model, compared with the present data (closed circle with error bars). The one-neutron separation energy for ^{37}Mg is an estimated value from Ref. [42]. The S_n value reported in [41] is shown with a gray zone. The insert shows the density distribution of ^{37}Mg at the expected separation energy $S_n = 0.16$ MeV.

central part of the DWS potential depth is varied to change the S_n with β_2 value fixed. There are two candidates for the β_2 value; one is the AMD β_2 value 0.36 for ^{37}Mg and the other is the AMD β_2 value 0.40 for ^{36}Mg. Here we simply take the former case since there is no essential difference between the two cases in the following discussion. In Fig. 3 the value and uncertainty of S_n, 0.16 ± 0.68 MeV [42], has been applied. The S_n value reported in [41] is shown with a gray zone as a reference. For both S_n values, the calculated results of the [321 1/2] orbital with a large p-wave component reproduce the present data quite well. The results of the f-dominant [312 5/2] orbital considerably underestimate the data for any value of S_n. This suggests that the ground state of ^{37}Mg might have a large [321 1/2] component.

To test possibilities of other orbitals for the valence neutron, the d-dominant [202 3/2] orbital was examined. The result (the dashed line in Fig. 3) also considerably underestimates the experimental value, similarly to the case of the f-dominant [321 1/2] orbital.

Only the σ_R for the p-dominant orbital increases steeply as S_n decreases. This behavior of the p-dominant orbital compared to the d- and f-dominant orbitals can come from the divergent nature of radii for orbitals with angular momenta $\ell \leqslant 1$ in the limit of $S_n \to 0$ [44]. From these results it can be concluded that the valence neutron should be in a p-dominant state.

The insert of Fig. 3 shows the density distribution of ^{37}Mg at $S_n = 0.16$ MeV where the valence neutron is in the p-dominant [321 1/2] orbital. This distribution shows a clear tail in the outer part, which can be referred to as a neutron halo. Using the p-dominant [321 1/2] orbital model, we can evaluate the rms radius of the nucleon distribution consistent with measured σ_R. The evaluated rms radius for ^{37}Mg is $3.65^{+0.09}_{-0.05}$ fm. Here, the evaluated rms radius of the valence neutron in [321 1/2] orbital is quite large: $7.83^{+1.6}_{-1.1}$ fm. The asymmetry in the errors is due to the strongly nonlinear relation between σ_R and the rms radii with changing S_n.

In the present DWS model, the f-dominant [312 5/2] orbital is lower in energy than the p-dominant [321 1/2] orbital at $\beta_2 = 0.36$. The parameter set of the DWS potential is determined so as to reproduce the spectroscopic properties of high spin states of light to heavy deformed stable nuclei. (See Ref. [45] for actual values of the parameters. It is natural to consider that the DWS potentials for unstable nuclei have larger diffuseness in the central and spin-orbit parts than those for stable nuclei.) Hence we investigate the sensitivity of the single-particle energies to the change of the diffuseness parameter. As a result, larger diffuseness values in the central and spin-orbit potentials make the p-dominant orbital lower in energy than the f-dominant orbital at $\beta_2 = 0.36$. About 30% enhancement of the standard value of 0.68 fm can explain the inversion of the orbitals at that deformation. This is explained by the fact that the p-dominant orbital wave function has a larger magnitude than the f-dominant one in the tail region where larger diffuseness makes the central part of the potential more attractive and the spin-orbit part weaker. Another possible origin of the inversion of these orbitals might be the tensor force effect [46]. Since the effect is not included in the DWS model, it is quite interesting to see whether the effect quantitatively explains the inversion of these orbitals at $\beta_2 = 0.36$.

While the enhancement of σ_R for ^{37}Mg can be explained by the neutron halo effect, for ^{38}Mg the measured σ_R is not enhanced from the theoretical result as shown in Fig. 1(a). This might be able to be attributed to the antihalo effect proposed by Hagino and Sagawa [47]. Due to this effect the separation energy of valence neutron(s) might not be so small for ^{38}Mg despite that nucleus being more neutron-rich than ^{37}Mg. Actually, the estimated value of the two-neutron (one-neutron) separation energy for ^{38}Mg is 2.4 ± 0.7 (2.3 ± 0.7) MeV [42].

In summary, we have measured σ_R for $^{24-38}$Mg on ^{12}C targets at energies around 240 MeV/nucleon. An enhancement of σ_R compared to the systematics of stable nuclei has been observed over the whole mass range. This enhancement is well explained by the double-folding model (DFM) calculation with the deformation effect extracted from the antisymmetrized molecular dynamics (AMD) calculation. However, the prominent enhancement observed for ^{37}Mg could not be accounted for by only the deformation but could be explained by a DFM calculation based on the deformed Woods-Saxon (DWS) model with the valence neutron in the p-dominant Nilsson orbital [321 1/2]. This result implies halo formation based on a well-deformed nuclear structure leading to the collapse of the $N = 28$ magic shell closure for neutrons in ^{37}Mg. Similar "deformed halo" phenomena have been seen for Ne isotopes [23,24] around the $N = 20$ shell. From the analysis

in this work, this phenomenon seems to emerge in the region beyond the island of inversion with a breakdown of the $N = 28$ shell closure. The mechanism which drives the break down of the $N = 28$ shell closure and nuclear deformation in this region should be investigated by further experimental and theoretical studies.

The authors thank the accelerator staff of the RIKEN Nishina Center for providing the intense ^{48}Ca beam and also thank Dr. J. Miller at LBNL for his careful reading of the manuscript. We thank Prof. M. Ishihara for fruitful discussions. This work was supported by JSPS KAKENHI Grants No. 22740186 and No. 24244024.

[1] O. Sorlin and M. G. Porque, Prog. Part. Nucl. Phys. **61**, 602 (2008).
[2] C. Thibault *et al.*, Phys. Rev. C **12**, 644 (1975).
[3] C. Détraz *et al.*, Phys. Rev. C **19**, 164 (1979).
[4] B. H. Wildenthal and W. Chung, Phys. Rev. C **22**, 2260 (1980).
[5] A. Watt, R. P. Singhal, M. H. Storm, and R. R. Whitehead, J. Phys. G **7**, L145 (1981).
[6] E. K. Warburton, J. A. Becker, and B. A. Brown, Phys. Rev. C **41**, 1147 (1990).
[7] P. Doornenbal *et al.*, Phys. Rev. Lett. **103**, 032501 (2009), and references therein.
[8] O. Sorlin *et al.*, Phys. Rev. C **47**, 2941 (1993).
[9] T. Glasmacher *et al.*, Phys. Lett. B **395**, 163 (1997).
[10] H. Scheit *et al.*, Phys. Rev. Lett. **77**, 3967 (1996).
[11] R. W. Ibbotson, T. Glasmacher, P. F. Mantica, and H. Scheit, Phys. Rev. C **59**, 642 (1999).
[12] F. Sarazin *et al.*, Phys. Rev. Lett. **84**, 5062 (2000).
[13] D. Sohler *et al.*, Phys. Rev. C **66**, 054302 (2002).
[14] L. Gaudefroy *et al.*, Phys. Rev. C **78**, 034307 (2008).
[15] M. Kimura, Y. Taniguchi, Y. Kanada-En'yo, H. Horiuchi, and K. Ikeda, Phys. Rev. C **87**, 011301 (2013).
[16] I. Hamamoto, Phys. Rev. C **85**, 064329 (2012).
[17] Y. Utsuno, T. Otsuka, B. A. Brown, M. Honma, T. Mizusaki, and N. Shimizu, Phys. Rev. C **86**, 051301 (2012).
[18] G. A. Lalazissis, D. Vretenar, P. Ring, M. Stoitsov, and L. M. Robledo, Phys. Rev. C **60**, 014310 (1999).
[19] B. Bastin *et al.*, Phys. Rev. Lett. **99**, 022503 (2007).
[20] S. Takeuchi *et al.*, Phys. Rev. Lett. **109**, 182501 (2012).
[21] P. Doornenbal *et al.*, Phys. Rev. Lett. **111**, 212502 (2013), and references therein.
[22] I. Tanihata *et al.*, Phys. Rev. Lett. **55**, 2676 (1985).
[23] M. Takechi *et al.*, Phys. Lett. B **707**, 357 (2012).
[24] T. Nakamura *et al.*, Phys. Rev. Lett. **103**, 262501 (2009).
[25] I. Hamamoto, Phys. Rev. C **81**, 021304(R) (2010).
[26] K. Minomo, T. Sumi, M. Kimura, K. Ogata, Y. R. Shimizu, and M. Yahiro, Phys. Rev. C **84**, 034602 (2011).
[27] K. Minomo, T. Sumi, M. Kimura, K. Ogata, Y. R. Shimizu, and M. Yahiro, Phys. Rev. Lett. **108**, 052503 (2012).
[28] T. Sumi, K. Minomo, S. Tagami, M. Kimura, T. Matsumoto, K. Ogata, Y. R. Shimizu, and M. Yahiro, Phys. Rev. C. **85**, 064613 (2012).
[29] T. Kubo, Nucl. Instrum. Methods B **204**, 97 (2003).
[30] T. Ohnishi *et al.*, J. Phys. Soc. Jpn. **77**, 083201 (2008).
[31] M. Fukuda *et al.*, Nucl. Phys. A **656**, 209 (1999).
[32] M. Takechi *et al.*, Phys. Rev. C **79**, 061601(R) (2009).
[33] S. Kox *et al.*, Phys. Rev. C **35**, 1678 (1987).
[34] K. Amos, P. Dortmans, H. von Geramb, S. Karataglidis, and J. Raynal, *Advances in Nuclear Physics*, Vol. 25 (Plenum, New York, 2000), p. 275.
[35] J. F. Berger, M. Girod, and D. Gogny, Comput. Phys. Commun. **63**, 365 (1991).
[36] M. Kimura and H. Horiuchi, Prog. Theor. Phys. **107**, 33 (2002).
[37] M. Seidlitz *et al.*, Phys. Lett. B **700**, 181 (2011).
[38] W. Horiuchi, T. Inakura, T. Nakatsukasa, and Y. Suzuki, Phys. Rev. C **86**, 024614 (2012).
[39] N. Kobayashi *et al.*, Few Body Syst. **54**, 1441 (2013).
[40] N. Kobayashi *et al.*, J. Phys. **436**, 012047 (2013).
[41] N. Kobayashi *et al.*, Phys. Rev. Lett. **112**, 242501 (2014).
[42] G. Audi *et al.*, Chin. Phys. C **36**, 1157 (2012).
[43] I. Hamamoto, Phys. Rev. C **76**, 054319 (2007).
[44] K. Riisager, A. S. Jensen, and P. Møller, Nucl. Phys. A **548**, 393 (1992).
[45] T. Shoji and Y. Shimizu, Prog. Theor. Phys. **121**, 319 (2009).
[46] T. Otsuka *et al.*, Phys. Rev. Lett. **104**, 012501 (2010).
[47] K. Hagino and H. Sagawa, Phys. Rev. C **84**, 011303(R) (2011).